Preprint
UCRL-JC-141881

Implicit Solution of Large-Scale Radiation Diffusion Problems

P. N. Brown, F. Graziani, I. Otero, C. S. Woodward

This article was submitted to
Nuclear Explosives Code Developers Conference, Oakland, CA,
October 23-27, 2001

January 4, 2001

U.S. Department of Energy

Lawrence
Livermore
National
Laboratory

Implicit Solution of Large-Scale Radiation Diffusion Problems (U)

Peter N. Brown, Frank Graziani, Ivan Otero, Carol S. Woodward
Lawrence Livermore National Laboratory

In this paper, we present an efficient solution approach for fully implicit, large-scale, nonlinear radiation diffusion problems. The fully implicit approach is compared to a semi-implicit solution method. Accuracy and efficiency are shown to be better for the fully implicit method on both one- and three-dimensional problems with tabular opacities taken from the LEOS opacity library. (U)

Keywords: radiation diffusion, implicit, preconditioners, time integration

Introduction

In this paper, we present a solution method for fully implicit radiation diffusion problems discretized on meshes having millions of spatial zones. This solution method makes use of high order in time integration techniques, inexact Newton–Krylov nonlinear solvers, and multigrid preconditioners. We explore the advantages and disadvantages of the fully implicit method as compared to a semi-implicit scheme on both one- and three-dimensional problems with tabulated opacities.

Research in the area of solution methods for fully implicit radiation diffusion has been active in the last few years. Knoll, Rider, and Olson (1998) showed that the fully implicit form of the one-dimensional radiation diffusion problem with analytic opacities gave greater accuracy in shorter times than did traditional methods. Later work by these authors showed that a fully implicit method with second order time-stepping leads to greater accuracy gains than first order fully implicit (Knoll, et al., 2000). Recent work by Mousseau, Knoll, and Rider (1999) has considered the fully implicit formulation of radiation diffusion using an operator splitting preconditioner. They saw this preconditioner to be quite effective in solving one- and two-dimensional problems. In previous work (Brown and Woodward, 2000), we have addressed issues related to the development of effective solvers for large-scale, three-dimensional, fully implicit radiation problems. We found that preconditioners for the implicit system need to account for the coupling between matter and radiation effectively. We also showed that the choice of preconditioner is crucial to the success of the fully implicit solve for large-scale problems.

One criticism of fully implicit solution approaches is that opacity evaluations, which are required more frequently in this approach than in semi-implicit formulations, can seem prohibitively expensive for the method. Previous work on fully implicit formulations has not addressed this issue. In this paper, we present our solution method and compare its advantages and disadvantages to that of a semi-implicit method for large, three-dimensional problems with tabulated opacities from the LEOS equation of state library (Corey and Young, 1997). Our results indicate that a fully implicit solution approach can achieve more accurate solutions than semi-implicit solution methods in many simulations involving the interaction of radiation and matter. Furthermore, the fully implicit approach can be as cost effective as semi-implicit approaches in many cases.

In the next section of this paper, we outline the model problem we are considering. The following section overviews both the fully implicit and semi-implicit solution methods we

employ, as well as the nonlinear and linear solvers we use. The results section gives some numerical results comparing the two methods. Lastly, the final section gives some conclusions about the viability of fully implicit methods on radiation diffusion problems.

Radiation Diffusion Model

For this work, we consider the flux-limited, two-temperature formulation of radiation diffusion given by

$$\frac{\partial E_R}{\partial t} = \nabla \cdot \left(\frac{c}{3\rho\kappa_R(T_R) + \frac{\|\nabla E_R\|}{E_R}} \nabla E_R \right) + c\rho\kappa_P(T_M) \cdot \left(aT_M^4 - E_R \right) + \chi(\mathbf{x}) c a T_{\text{source}}^4, \tag{1}$$

where $E_R(\mathbf{x}, t)$ is the radiation energy density ($\mathbf{x} = (x, y, z)$), $T_M(\mathbf{x}, t)$ is the material temperature, $\rho(\mathbf{x})$ is the material density, c is the speed of light, and $a = 4\sigma/c$ where σ is the Stephan–Boltzmann constant. The Rosseland opacity, κ_R, is a nonlinear function of the radiation temperature, T_R, which is defined by the relation $E_R = aT_R^4$. The Planck opacity, κ_P, is a nonlinear function of material temperature, T_M, which is related to the material energy through an equation of state, $E_M = \text{EOS}(T_M)$. Here, T_{source} is a given source temperature, and $\chi(\mathbf{x})$ is a function of the spatial variable $\mathbf{x}$. In the limiter, the norm $\|\cdot\|$ is just the l^2 norm of the gradient vector.

This equation is coupled to an equation expressing conservation of material energy given by

$$\frac{\partial E_M}{\partial t} = -c\rho\kappa_P(T_M) \cdot \left(aT_M^4 - E_R \right). \tag{2}$$

We consider Dirichlet, Neumann, and Robin boundary conditions for the system (1)–(2), and our focus here is on the development of solution methods for this system.

Solution Methods

For both the fully implicit and semi-implicit formulations, we employ a cell-centered finite difference approach for the spatial discretization. We use a tensor product grid with N_x, N_y, and N_z cells in the x, y, and z directions, respectively. Defining $E_{R,i,j,k}(t) \approx E_R(\mathbf{x}_{i,j,k}, t)$ and $E_{M,i,j,k}(t) \approx E_M(\mathbf{x}_{i,j,k}, t)$, with $\mathbf{x}_{i,j,k} = (x_i, y_j, z_k)$, and

$$\mathbf{E}_R \equiv \begin{pmatrix} E_{R,1,1,1} \\ \vdots \\ E_{R,N_x,N_y,N_z} \end{pmatrix} \text{ and } \mathbf{E}_M \equiv \begin{pmatrix} E_{M,1,1,1} \\ \vdots \\ E_{M,N_x,N_y,N_z} \end{pmatrix},$$

we can write our discrete equations in terms of a discrete diffusion operator given by $\mathbf{L}(\mathbf{E}_R) \equiv \left(L_{1,1,1}(\mathbf{E}_R), \cdots, L_{N_x,N_y,N_z}(\mathbf{E}_R) \right)^T$, and a local coupling operator given by $\mathbf{S}(\mathbf{E}_R, \mathbf{E}_M) \equiv (S_{1,1,1}(\mathbf{E}_R, \mathbf{E}_M), \cdots, S_{N_x,N_y,N_z}(\mathbf{E}_R, \mathbf{E}_M))^T$, where

$$L_{i,j,k}(\mathbf{E}_R) = \left(\frac{c}{3\rho_{i+1/2,j,k}\kappa_{R,i+1/2,j,k} + \frac{\|\nabla E_R\|_{i+1/2,j,k}}{E_{R,i+1/2,j,k}}} \frac{E_{R,i+1,j,k} - E_{R,i,j,k}}{\Delta x_{i+1/2,j,k}} \right.$$

$$\left. -\frac{c}{3\rho_{i-1/2,j,k}\kappa_{R,i-1/2,j,k} + \frac{\|\nabla E_R\|_{i-1/2,j,k}}{E_{R,i-1/2,j,k}}} \frac{E_{R,i,j,k} - E_{R,i-1,j,k}}{\Delta x_{i-1/2,j,k}} \right) / \Delta x_i \qquad (3)$$

$+$ y and z terms,

and

$$S_{i,j,k}(E_{R,i,j,k}, E_{M,i,j,k}) = c\rho_{i,j,k}\kappa_{P,i,j,k}\left(aT^4_{M,i,j,k} - E_{R,i,j,k}\right). \qquad (4)$$

Thus, our discrete scheme is to find $\mathbf{E}_R(t)$ and $\mathbf{E}_M(t)$ such that,

$$\frac{d\mathbf{E}_R}{dt} = \mathbf{L}(\mathbf{E}_R) + \mathbf{S}(\mathbf{E}_R, \mathbf{E}_M) + \mathbf{Q}, \qquad (5)$$

$$\frac{d\mathbf{E}_M}{dt} = -\mathbf{S}(\mathbf{E}_R, \mathbf{E}_M), \qquad (6)$$

where $\mathbf{Q}$ includes the source term along with terms from the discretized boundary conditions. For more details, see Brown and Woodward (2000).

Fully Implicit Formulation. For the fully implicit formulation, we use an ODE time integrator to handle the implicit time step selection for the system (5)-(6). In particular, we employ the parallel ODE solver, PVODE (Byrne and Hindmarsh, 1999), developed at Lawrence Livermore National Laboratory and based on the VODPK package (Byrne, 1992). PVODE employs the fixed leading coefficient variant of the Backward Differentiation Formula (BDF) method (Brown et al., 1989, Jackson and Sacks-Davis, 1980) and allows for variation in the order of the time discretization as well as in the time step size.

The methods in PVODE are Predictor-Corrector in nature, so each time step begins with the calculation of an explicit predictor. An implicit corrector is then employed to solve for the time step solution. This time integration technique leads to a coupled, nonlinear system of equations that must be solved at each time step. For example, solving the ODE system

$$\dot{y} = f(t, y), \qquad (7)$$

with the backward Euler method (i.e., the BDF method of order 1), leads to the following nonlinear system

$$0 = F(y) \equiv y - \Delta t f(t_n, y) - y_{n-1} \quad \left(\text{i.e.,} \frac{y_n - y_{n-1}}{\Delta t} = f(t_n, y_n)\right) \qquad (8)$$

that must be solved for $y = y_n$ at each time step. For the solution of this system, we use an inexact Newton–Krylov method with Jacobian-vector products approximated by finite differences of the form

$$F'(y)v \approx \frac{F(y + \theta v) - F(y)}{\theta}, \qquad (9)$$

where θ is a scalar. Within the Newton–Krylov paradigm, only the implementation of the nonlinear function is necessary, and Jacobian matrix entries need never be formed or stored. Heuristic arguments for the case of systems arising from the implicit integration of ODEs show that $\theta = 1$ works quite well (Brown and Hindmarsh, 1986) and is the choice used in

PVODE. Finally, the explicit predictor, $y_{n(0)}$, is used as an initial guess to the nonlinear system (8).

In the methods discussed above, we use the scaling technique incorporated into PVODE. Thus, we include an absolute tolerance (ATOL) for each unknown and a relative tolerance (RTOL) applied to all unknowns. These tolerances are then used to form a weight that is applied to each solution component during the time step from t_{n-1} to t_n. This weight is given as

$$w_i = \text{RTOL} \cdot |y^i_{n-1}| + \text{ATOL}_i, \tag{10}$$

and then the weighted root mean square norm

$$\|y\|_{\text{WRMS}} = \left[N^{-1} \sum_{i=1}^{N} (y_i/w_i)^2\right]^{1/2} \tag{11}$$

is applied on all error-like vectors within the solution process. This scaling gives each solution component equal weight when measuring the size of or errors in y. For our application, we supply two absolute tolerances, one to be used with the radiation energy unknowns and one to be used with the material energy unknowns.

Time step sizes are chosen in an attempt to maximize step sizes while controlling the local truncation error, and thus give a solution that obeys a user-specified accuracy bound. The local truncation error can, in general, only be estimated, and so PVODE uses the estimate

$$LTE(\Delta t^n) \equiv C_q(y_n - y_{n(0)}), \tag{12}$$

where y_n is the final iterate in the Newton iteration and C_q is a constant that depends on the BDF method order q but is independent of the solution. If $\|LTE(\Delta t^n)\|_{\text{WRMS}} < 1$, then the time step is accepted. If this condition is violated, the step size is cut, and the solution is recomputed. New steps are chosen by estimating the local truncation error at the new step, $\Delta t'$, as

$$\|LTE(\Delta t')\|_{\text{WRMS}} \approx \left(\frac{\Delta t'}{\Delta t^n}\right)^{q+1} \|LTE(\Delta t)\|_{\text{WRMS}}, \tag{13}$$

where q is the current method order. The new step is chosen to give the largest time step still satisfying $\|LTE(\Delta t')\|_{\text{WRMS}} < 1$. PVODE also changes the BDF method order by comparing the local truncation errors for the BDF methods of order $q-1$ and $q+1$ when using order q, and then taking the order that allows the largest time step.

We use the GMRES Krylov iterative solver for solution of the linear Jacobian system at each Newton iteration (Saad and Schultz, 1986). The tolerance for the Newton iteration is taken to guarantee that iteration error introduced from the nonlinear solver is smaller than the local truncation error. The default linear system tolerance in PVODE is taken to be the factor $\alpha = 0.05$ times the nonlinear system tolerance. This factor can be optionally set in the PVODE solver, and for some of the problems discussed below we use a smaller value of α, as the default of 0.05 did not work for the larger RTOL values. The default maximum subspace dimension for GMRES in PVODE is 5, and we use this default in all of our tests.

Preconditioning is generally essential when using Krylov linear solvers. To describe our preconditioning strategy, we begin by considering the content and structure of the Jacobian

matrix. In (7), set $y = (\mathbf{E}_R^T, \mathbf{E}_M^T)^T$, and then form f using the right-hand sides of (5)-(6). The Jacobian matrices used in the Newton method are of the general form $F'(y) = (I - \gamma J)$, where $J = \partial f/\partial y$ is the Jacobian of the nonlinear function f, and the parameter $\gamma \equiv \Delta t \beta$ with Δt the current time step value and β a coefficient depending on the order of the BDF method. Recalling the definitions of the discrete divergence and source operators, the block form of the Jacobian of f is

$$J = \begin{pmatrix} \partial \mathbf{L}/\partial \mathbf{E}_R + \partial \mathbf{S}/\partial \mathbf{E}_R & \partial \mathbf{S}/\partial \mathbf{E}_M \\ -\partial \mathbf{S}/\partial \mathbf{E}_R & -\partial \mathbf{S}/\partial \mathbf{E}_M \end{pmatrix} = \begin{pmatrix} A+G & B \\ -G & -B \end{pmatrix},$$

where $A = \partial \mathbf{L}/\partial \mathbf{E}_R$, $G = \partial \mathbf{S}/\partial \mathbf{E}_R$, and $B = \partial \mathbf{S}/\partial \mathbf{E}_M$. We note that G and B are diagonal matrices.

On close inspection of the nonlinear diffusion operator $\mathbf{L}(\mathbf{E}_R)$, we can write

$$\mathbf{L}(\mathbf{E}_R) = \hat{\mathbf{L}}(\mathbf{E}_R)\mathbf{E}_R, \tag{14}$$

where $\hat{\mathbf{L}}$ is a nonlinear matrix-valued function of $\mathbf{E}_R$. In all of our preconditioning strategies, we neglect the nonlinearity in the diffusion term and use the approximation

$$A = \partial \mathbf{L}(\hat{\mathbf{E}}_R)/\partial \mathbf{E}_R \approx \hat{\mathbf{L}}(\hat{\mathbf{E}}_R) \equiv \tilde{A},$$

where $\partial \mathbf{L}(\hat{\mathbf{E}}_R)/\partial \mathbf{E}_R$ is the Jacobian of $\mathbf{L}$ evaluated at a radiation energy, $\hat{\mathbf{E}}_R$. The size of the neglected term is related to the derivatives of the Rosseland opacity and the flux-limiter. Our motivation for neglecting this term arises from the fact that $-\tilde{A}$ is symmetric and positive definite, whereas $-A$ is not. In addition, the derivative of the flux-limiter may lead to numerical errors if $\nabla \mathbf{E}_R$ approaches 0.

Our preconditioning strategy is to factor the matrix

$$\begin{pmatrix} P & Q \\ R & T \end{pmatrix} \equiv \begin{pmatrix} I - \gamma(\tilde{A}+G) & -\gamma B \\ \gamma G & I + \gamma B \end{pmatrix} = M$$

into the following:

$$M_{\text{Schur}} = \begin{pmatrix} I & QT^{-1} \\ 0 & I \end{pmatrix} \begin{pmatrix} P - QT^{-1}R & 0 \\ 0 & T \end{pmatrix} \begin{pmatrix} I & 0 \\ T^{-1}R & I \end{pmatrix}.$$

Letting $S = P - QT^{-1}R$, we write the solution to $M_{\text{Schur}}x = b$ as

$$\begin{pmatrix} x_1 \\ x_2 \end{pmatrix} = \begin{pmatrix} S^{-1}(b_1 - QT^{-1}b_2) \\ T^{-1}(-Rx_1 + b_2) \end{pmatrix}.$$

If the Schur complement, S, is exactly inverted, there will be no error associated with this preconditioner for the non-flux-limited, constant opacity case. In addition, because B and hence T is diagonal, there is no penalty associated with inverting T for every iteration of a method that inverts S, as there would be if a material energy diffusion term were added to the equations. Also note that S is formed by modifying the diagonal of P. Hence, we can employ multigrid methods to invert this Schur complement.

The Rosseland opacity will exhibit large changes where material interfaces exist in the domain. The temperature dependence gives rise to large value changes as well. These

changes imply that the problem can be very heterogeneous. As a result, to invert matrix blocks formed from the diffusion operator, we use a multigrid method designed to handle large changes in problem coefficients. In particular, we use one V-cycle of the SMG algorithm developed by Schaffer (Schaffer, 1998 and Brown et al., 2000) as our multigrid solver. Other multigrid methods have been developed for highly heterogeneous problems. A comparison of SMG and another of these methods can be found in Jones and Woodward (2000). We use SMG here because it is highly robust and scales extremely well. Details of the SMG method can be found in the cited references. More information about multigrid methods in general can be found in Briggs et al. (2000).

Since Jacobian approximations can be expensive to compute, the preconditioner is not updated with every Newton iteration. Preconditioner updates occur only when the Newton iteration fails to converge, 20 time steps pass without an update, or when there is a significant change in the time step size and order of the ODE method.

In summary, the main advantage of the fully implicit method is that we have accurate error control in the time step selection process allowing step sizes to automatically adjust to the problem physics while maintaining accuracy. The main disadvantage of the method is that opacities must be calculated for every linear iteration, as a nonlinear function evaluation is required in the matrix-vector product approximation (9). In general, fully implicit methods require more sophisticated solvers than semi-implicit methods. The solution method presented above has been tested on very large, three-dimensional problems and has been shown to be parallel scalable up to almost 6,000 processors (Brown and Woodward, 2000).

Semi-Implicit Method. The semi-implicit method we compare against was developed to match traditional methods. In this formulation, a backward Euler time stepping technique is applied, opacities and flux-limiters are evaluated at the start of a new time step using the solution from the previous step, and the coupling term is linearized about the solution from the previous step. The problem is put in a residual formulation so that the single linear solve required at each time step gives the increment to the solution values from the previous step's solution.

Beginning with the discrete system (5)–(6) and using (14), we can write

$$\frac{\mathbf{E}_R^{n+1} - \mathbf{E}_R^n}{\Delta t} = \hat{\mathbf{L}}(\mathbf{E}_R^n)\mathbf{E}_R^{n+1} + \mathbf{K}(\mathbf{T}_M^n)(a(\mathbf{T}_M^{n+1})^4 - \mathbf{E}_R^{n+1}) + \mathbf{Q}^{n+1}, \tag{15}$$

$$\frac{\mathbf{E}_M^{n+1} - \mathbf{E}_M^n}{\Delta t} = -\mathbf{K}(\mathbf{T}_M^n)(a(\mathbf{T}_M^{n+1})^4 - \mathbf{E}_R^{n+1}), \tag{16}$$

where $\mathbf{K}(\mathbf{T}_M^n)$ is a diagonal matrix whose entries are given by $K_{i,j,k} \equiv c\rho\kappa_P(T_{M,i,j,k}^n)$ and $E_{M,i,j,k}^{n+1} = \mathrm{EOS}(T_{M,i,j,k}^{n+1})$. Next, letting $\mathbf{T}_M^{n+1} = \mathbf{T}_M^n + \boldsymbol{\Delta}\mathbf{T}_M^n$ we linearize to obtain

$$(\mathbf{T}_M^{n+1})^4 = (\mathbf{T}_M^n + \boldsymbol{\Delta}\mathbf{T}_M^n)^4 \approx (\mathbf{T}_M^n)^4 + 4(\mathbf{T}_M^n)^3\boldsymbol{\Delta}\mathbf{T}_M^n.$$

Similarly, we linearize $E_M = \mathrm{EOS}(T_M)$ to obtain

$$\mathbf{E}_M^{n+1} = \mathbf{EOS}(\mathbf{T}_M^n + \boldsymbol{\Delta}\mathbf{T}_M^n) \approx \mathbf{EOS}(\mathbf{T}_M^n) + \frac{\partial \mathbf{EOS}}{\partial \mathbf{T}_M}(\mathbf{T}_M^n)\boldsymbol{\Delta}\mathbf{T}_M^n,$$

or

$$\mathbf{E}_M^{n+1} - \mathbf{E}_M^n \approx \frac{\partial \mathbf{EOS}}{\partial \mathbf{T}_M}(\mathbf{T}_M^n)\Delta\mathbf{T}_M^n.$$

Thus,

$$(\mathbf{T}_M^{n+1})^4 \approx (\mathbf{T}_M^n)^4 + 4(\mathbf{T}_M^n)^3 \left[\frac{\partial \mathbf{EOS}}{\partial \mathbf{T}_M}(\mathbf{T}_M^n)\right]^{-1} (\mathbf{E}_M^{n+1} - \mathbf{E}_M^n).$$

Substituting this last relationship into (15)–(16), we have

$$\begin{aligned} \mathbf{E}_R^{n+1} - \mathbf{E}_R^n &= \Delta t\hat{\mathbf{L}}(\mathbf{E}_R^n)\mathbf{E}_R^{n+1} + \Delta t\mathbf{K}(\mathbf{T}_M^n)\cdot \\ &\left(a\left[(\mathbf{T}_M^n)^4 + 4(\mathbf{T}_M^n)^3\left[\frac{\partial \mathbf{EOS}}{\partial \mathbf{T}_M}(\mathbf{T}_M^n)\right]^{-1}(\mathbf{E}_M^{n+1} - \mathbf{E}_M^n)\right] - \mathbf{E}_R^{n+1}\right) + \Delta t\mathbf{Q}^{n+1}, \end{aligned} \tag{17}$$

$$\begin{aligned} \mathbf{E}_M^{n+1} - \mathbf{E}_M^n &= -\Delta t\mathbf{K}(\mathbf{T}_M^n)\cdot \\ &\left(a\left[(\mathbf{T}_M^n)^4 + 4(\mathbf{T}_M^n)^3\left[\frac{\partial \mathbf{EOS}}{\partial \mathbf{T}_M}(\mathbf{T}_M^n)\right]^{-1}(\mathbf{E}_M^{n+1} - \mathbf{E}_M^n)\right] - \mathbf{E}_R^{n+1}\right), \end{aligned} \tag{18}$$

where we solve for the changes, $\mathbf{\Delta E}_R^n \equiv \mathbf{E}_R^{n+1} - \mathbf{E}_R^n$ and $\mathbf{\Delta E}_M^n \equiv \mathbf{E}_M^{n+1} - \mathbf{E}_M^n$, given the previous values of $\mathbf{E}_R^n$ and $\mathbf{E}_M^n$.

We solve the linear system (17)–(18) using the same linear solver as described above: the GMRES Krylov iterative solver with a Schur complement factorization preconditioner. The same multigrid method is used to invert the Schur complement matrix as in the fully implicit case. The linear iteration is performed until the relative residual is bounded by an input tolerance times the norm of the right-hand side,

$$\|\mathbf{r}\|_{\text{WRMS}} \leq \epsilon\|\mathbf{b}\|_{\text{WRMS}}, \tag{19}$$

where $\mathbf{r}$ is the linear system residual, $\mathbf{b}$ is the linear system right-hand side, and ϵ is an input parameter. The WRMS norm is calculated in the same way as that for PVODE, using RTOL and ATOL values chosen as in the PVODE case.

Time steps are chosen to try to restrict changes in radiation energy and material temperature within a step. For specified minimum values, $E_{\min}$ and $T_{\min}$, and specified fractional variations allowed in a step, E_{frac} and T_{frac}, the new step is computed by first calculating a maximum variation for each variable,

$$v_R = \max_{i,j,k}\left(\frac{\Delta E_R^n}{0.5(E_R^{n-1} + E_R^n) + E_{\min}}\right), \quad v_M = \max_{i,j,k}\left(\frac{\Delta T_M^n}{0.5(T_M^{n-1} + T_M^n) + T_{\min}}\right). \tag{20}$$

Then, the new step is chosen as

$$\Delta t^{\text{new}} = \Delta t^{\text{old}} \cdot \min(E_{\text{frac}}/(v_R + \delta), T_{\text{frac}}/(v_M + \delta)), \tag{21}$$

where $\delta = 10^{-7}$ limits the maximum change in the step size. Note that this selection process is similar to the error control for the fully implicit case. However, while the semi-implicit approach bounds the maximum change in solution components over a time step, the fully

implicit approach is bounding the maximum local truncation error made on a step with no direct control on the solution components. Finally, if the linear iteration fails to converge, then the step is repeated with $\Delta t^{\text{new}} = 0.5 \cdot \Delta t^{\text{old}}$.

Numerical Results

We consider three problems. The first problem is a one-dimensional problem from Su and Olson (1996), and is an excellent test problem in that they provide an analytic solution to compare results against. The second problem is a one-dimensional Marshak wave problem using tabulated opacities, while the third is a three-dimensional internal source problem. In the tables below,

PVODE	=	PVODE was used as the solver,
S-Imp	=	the semi-implicit solver was used,
RTOL	=	the RTOL value used,
ORD	=	the maximum order allowed for PVODE, and
FRAC	=	the $E_{\text{frac}} (= T_{\text{frac}})$ value used,

and the statistical counters are

NST	=	total number of time steps,
NNI	=	total number of nonlinear iterations,
NLI	=	total number of linear iterations,
NFE	=	total number of $f(t, y)$ evaluations,
NPE	=	total number of preconditioner evaluations,
NPS	=	total number of preconditioner solves,
RT	=	run time in seconds.

All runs done with PVODE allowed a BDF method of order up to 2 unless specified as order 1. In this case, BDF methods of order 1 only were allowed.

Su–Olson Test Problem. As this problem has an analytic solution, we have verified that our numerical results for both methods converge to the true solution as the spatial mesh is refined and tolerances for time stepping are tightened. Thus, as both methods are accurate we focus on the efficiency and robustness of the two approaches in the following two problems.

One-Dimensional Marhsak Wave Problem. We give results of using the two solution approaches on a one-dimensional Marshak wave problem involving the use of tabular opacities. We use the LEOS (Corey and Young, 1997) package to give the Rosseland and Planck opacities as nonlinear functions of the radiation temperature T_R and material temperature T_M, respectively. The system (1)–(2) is solved on the box $\mathcal{D} \equiv \{\mathbf{x} = (x, y, z) : 0 \leq x, y, z \leq 1\text{cm}\}$ with Dirichlet boundary conditions at $x = 0$ and $x = 1$, and homogeneous Neumann boundary conditions on the other faces. The function $\chi(\mathbf{x})$ in (1) is identically zero for this problem. The left Dirichlet boundary condition for the radiation energy density was $E_{R,\text{left}} = aT_{R,\text{left}}^4$, where $T_{R,\text{left}} = 3,481,440\ ^\circ K$ (approximately $300eV$), the initial conditions were taken as $E_R = aT_{R,0}^4$ and $E_M = EOS(\rho, T_{M,0})$, where $T_{R,0} = T_{M,0} = 300\ ^\circ K$. The right Dirichlet boundary value for E_R is taken to be consistent with the initial condition. The material used was carbon at a reference density of $\rho = 1.05 g/cc$. The spatial grid was uniform with $N_x = 80, N_y = N_z = 1$. While several values of RTOL are used, only one

set of ATOL values was used for all the problems in this section. For the radiation energy density, an ATOL value of $\text{ATOL}_R = aT^4_{R,\text{ATOL}}$ was used, where $T_{R,\text{ATOL}} = 200\ ^\circ K$, and for the material energy density an ATOL value of $\text{ATOL}_M = 200\ ^\circ K$ was used. A value of $\epsilon = 10^{-6}$ was used in (19), along with the values $E_{\text{min}} = T_{\text{min}} = 0.1keV$. Finally, a linear stopping tolerance factor of $\alpha = 0.01$ was used for all the PVODE runs.

For this problem, the time behavior consists of an initial transient in which the material heats up in the region of the left boundary (from 0 to .02 microseconds), followed by a radiation front traveling to the right boundary (continuing to 1 microsecond), and then a final phase in which the solution approaches a steady state. Figures 1, 2, 3, and 4 show the solutions and relative errors (as compared to the PVODE solution using $\text{RTOL} = 10^{-5}$) plotted at .016 microseconds. Figures 5 and 6 show the maximum relative errors (as compared to the PVODE solution using $\text{RTOL} = 10^{-5}$) in x plotted for each output point from 0 to .02 microseconds, while Figures 7 and 8 show the same values for the interval from 0.4 to 0.5 microseconds. Table 1 compares the statistics of the two solvers when integrating the problem from 0 to 1 microsecond.

As can be seen from the plots and the table, the PVODE solution obtained using $\text{RTOL} = 10^{-3}$ with a maximum order of 1 give errors roughly equivalent to the semi-implicit solution using $E_{\text{frac}} = T_{\text{frac}} = 0.1$. However, the run time for the PVODE solver is only 65% that of the semi-implicit solver. Also, the PVODE solution with $\text{RTOL} = 10^{-4}$ and maximum order 2 is at least 1 order of magnitude more accurate than the semi-implicit solution with FRAC= 0.1, and at the same time it is faster. It is also interesting to note that the potentially more accurate semi-implicit solution using FRAC= 0.01 is actually the least accurate for the larger output times. This is due to the accumulation of roundoff errors, as there is a prohibitively large number of steps when using the tighter FRAC value.

Table 1: Solver statistics for one-dimensional Marshak wave problem

Method	NST	NNI	NLI	NPE	NPS	RT	RTOL	ORD	FRAC
PVODE	7146	9736	15135	1102	24861	125	1.e-3	2	–
PVODE	17532	26295	33533	3968	59811	325	1.e-4	2	–
PVODE	38048	53683	69301	8932	122924	679	1.e-5	2	–
PVODE	19270	21385	41583	1194	62949	281	1.e-3	1	–
PVODE	61005	68499	122693	4452	191165	875	1.e-4	1	–
S-Imp	13348	–	36087	13352	49435	431	1.e-4	–	0.1
S-Imp*	106643	–	305017	106643	411660	>3600	1.e-4	–	0.01

*(computed only 634 of 1000 output snapshots in 3600 seconds)

Three-Dimensional Source Problem. In this problem, the system (1)–(2) is solved on the box $\mathcal{D} \equiv \{\mathbf{x} = (x, y, z) : 0 \le x, y, z \le 1cm\}$ with Dirichlet boundary conditions. The function $\chi(\mathbf{x})$ in (1) is defined by

$$\chi(\mathbf{x}) = \begin{cases} 1, \text{ if } 0.45 \le x, y, z \le 0.55, \text{ and} \\ 0, \text{ otherwise.} \end{cases} \tag{22}$$

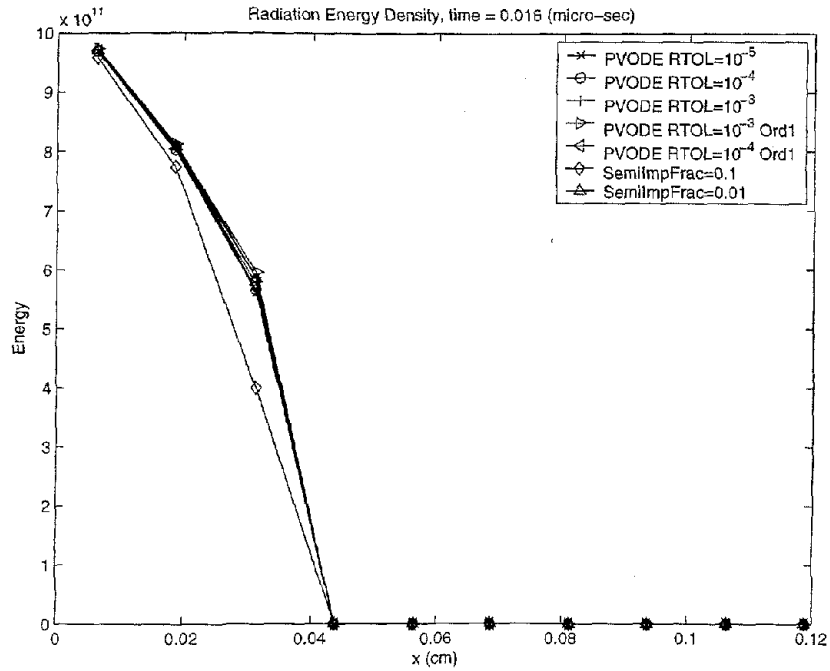

Figure 1: Radiation energy density for one-dimensional Marshak wave

The parameter T_{source} was $3keV$ and the initial conditions were taken as $E_R = aT_{R,0}^4$ and $E_M = EOS(\rho, T_{M,0})$, where $T_{R,0} = T_{M,0} = 8.616976eV$ (approximately $10,000\ ^\circ K$). The boundary conditions are taken to be consistent with the initial conditions. The material used was carbon at a reference density of $\rho = 0.00893g/cc$. The spatial grid was uniform with $N_x = N_y = N_z = 80$. While several values of RTOL are used, only one set of ATOL values was used for all the problems in this section. For the radiation energy density, an ATOL value of $\text{ATOL}_R = aT_{R,\text{ATOL}}^4$ was used, where $T_{R,\text{ATOL}} = 0.01643keV$, and for the material energy density an ATOL value of $\text{ATOL}_M = 0.01keV$ was used. A value of $\epsilon = 10^{-6}$ was used in (19), along with the values $E_{\min} = \text{ATOL}_R$ and $T_{\min} = 0.01keV$. Finally, the default linear stopping tolerance factor of $\alpha = 0.05$ was used for all the PVODE runs.

Table 2 shows the statistics for this run. The problem was integrated from 0 to $5.2 \cdot 10^{-7}$ microseconds. The time behavior consists of an initial transient in which the material heats up in the region of the source, followed by a radiation front traveling to the boundary, and then a final phase in which the solution approaches a steady state. Figures 9 and 10 show the solutions plotted along the line $y = z = 0.5$cm at the final time (which is very early in the overall time behavior of the solution). Figures 11 and 12 show the maximum relative errors (as compared to the PVODE solution using RTOL $= 10^{-5}$) in x plotted for each output point from 0 to the final time. The 10^{-3} tolerance PVODE solution appears to be less accurate early in the simulation than the semi-implicit solution, and then the two achieve about the same accuracy for later times. However, the 10^{-3} tolerance PVODE run time is an order of magnitude cheaper than the semi-implicit approach. In addition, we see that the 10^{-4} tolerance PVODE run gives about an order of magnitude more accurate relative errors than the semi-implicit run and requires about half the run time than the semi-implicit run.

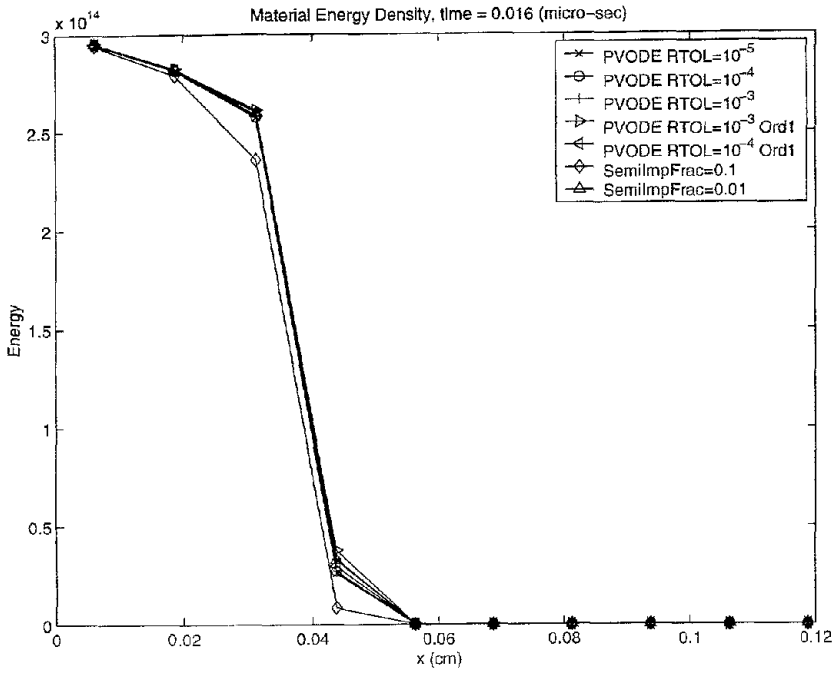

Figure 2: Material energy density for one-dimensional Marshak wave

Table 2: Solver statistics for three-dimensional source problem

Method	NST	NNI	NLI	NPE	NPS	RT	RTOL	ORD	FRAC
PVODE	47	58	180	13	235	542	1.e-3	2	–
PVODE	165	287	1076	25	1360	2383	1.e-4	2	–
PVODE	3104	3249	6861	180	10106	13250	1.e-5	2	–
S-Imp	370	–	1324	370	1694	4434	1.e-4	–	0.1

Conclusions

In this paper, we have demonstrated the superior accuracy of a fully implicit solution approach to the radiation diffusion system (5)–(6) when compared to a standard semi-implicit time integration approach. We have incorporated the use of tabular opacities in our model in an effort to enhance the accuracy of our test problems as well as to evaluate the added costs of additional function evaluations in the fully implicit approach. While our testing is limited, these results indicate that a fully implicit solution approach is a viable, cost-effective option in many simulations involving the interaction of radiation and matter.

Acknowledgment

This work was performed under the auspices of the U.S. Department of Energy by University of California Lawrence Livermore National Laboratory under contract No. W-7405-ENG-48.

References

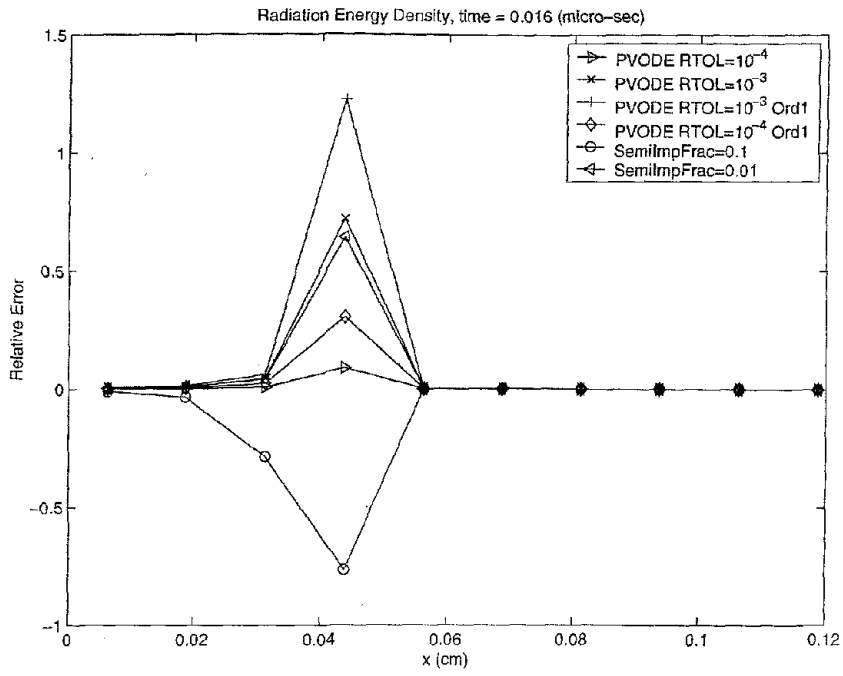

Figure 3: Radiation energy density relative error (measured against a PVODE run with RTOL= 10^{-5}) for one-dimensional Marshak wave

Briggs, W. F., Henson, V. E., and McCormick, S. F., *A Multigrid Tutorial, 2nd. Edition*, (SIAM, Philadelphia, PA, 2000).

Brown, P. N., Byrne, G. D., and Hindmarsh, A. C., "VODE: A Variable-Coefficient ODE Solver," *SIAM J. Sci. Stat. Comput.*, **10**, 1038–1051 (1989).

Brown, P. N., Falgout, R. D., and Jones, J. E., "Semicoarsening Multigrid on Distributed Memory Machines," *SIAM J. Sci. Comput.*, **21**, 1823–1834 (2000).

Brown, P. N., and Hindmarsh, A. C., "Matrix-Free Methods for Stiff Systems of ODE's," *SIAM J. Num. Anal.*, **23**, 610–638 (1986).

Brown, P. N., and Woodward, C. S., "Preconditioning Strategies for Fully Implicit Radiation Diffusion with Material-Energy Transfer," *SIAM J. Sci. Comput.* to appear. Also available as LLNL Technical Report UCRL-JC-139087, May 2000.

Byrne, G. D., "Pragmatic Experiments with Krylov Methods in the Stiff ODE Setting," *Computational Ordinary Differential Equations*, J. R. Cash and I. Gladwell, eds., (Oxford University Press, Oxford, 1992), p. 323–356.

Byrne, G. D., and Hindmarsh, A. C., "PVODE, An ODE Solver for Parallel Computers," *Int. J. High Perf. Comput. Appl.*, **13**, 354–365 (1999). Software available at: http://www.llnl.gov/CASC/PVODE/.

Corey, E. M., and Young, D. A., *A New Prototype Equation of State Data Library*, Lawrence Livermore National Laboratory, Livermore, CA, UCRL-JC-127698 (1997). Submitted to American Physical Society Meeting, 1997.

Jackson, K. R., and Sacks-Davis, R., "An Alternative Implementation of Variable Step-Size Multistep Formulas for Stiff ODEs," *ACM Trans. Math. Software*, **6**, 295–318 (1980).

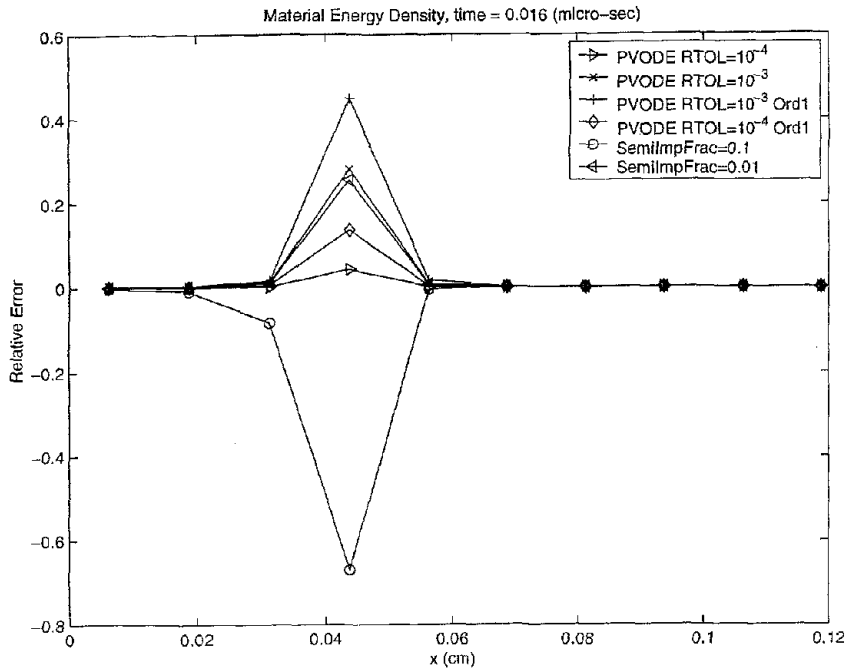

Figure 4: Material energy density relative error (measured against a PVODE run with RTOL= 10^{-5}) for one-dimensional Marshak wave

Jones, J. E., and Woodward, C. S., "Newton–Krylov-Multigrid Solvers for Large-Scale, Highly Heterogeneous, Variably Saturated Flow Problems," *Advances in Water Resources* to appear.

Knoll, D. A., Rider, W. J., and Olson, G. L., "An Efficient Nonlinear Solution Method for Nonequilibrium Radiation Diffusion," *J. Quant. Spec. and Rad. Trans.*, **63**, 15–29 (1999).

Knoll, D. A., Rider, W. J., and Olson, G. L., "Nonlinear Convergence, Accuracy, and Time Step Control in Nonequilibrium Radiation Diffusion," *J. Quant. Spec. and Rad. Trans.* to appear.

Mousseau, V. A., Knoll, D. A., and Rider, W. J., "Physics-Based Preconditioning and the Newton–Krylov Method for Non-Equilibrium Radiation Diffusion," *J. of Comput. Phys.*, **160**, 743–765 (2000).

Saad, Y., and Schultz, M. H., "GMRES: A Generalized Minimal Residual Algorithm for Solving Nonsymmetric Linear Systems," *SIAM J. Sci. Stat. Comput.*, **7**, 856–869 (1986).

Schaffer, S., "A Semicoarsening Multigrid Method for Elliptic Partial Differential Equations with Highly Discontinuous and Anisotropic Coefficients," *SIAM J. on Sci. Comp.*, **20**, 228–242 (1998).

Su, B., and Olson, G. L., "Benchmark results for the non-equilibrium Marshak diffusion problem," J. Quant. Spec. and Rad. Trans., **56**, 337–351 (1996).

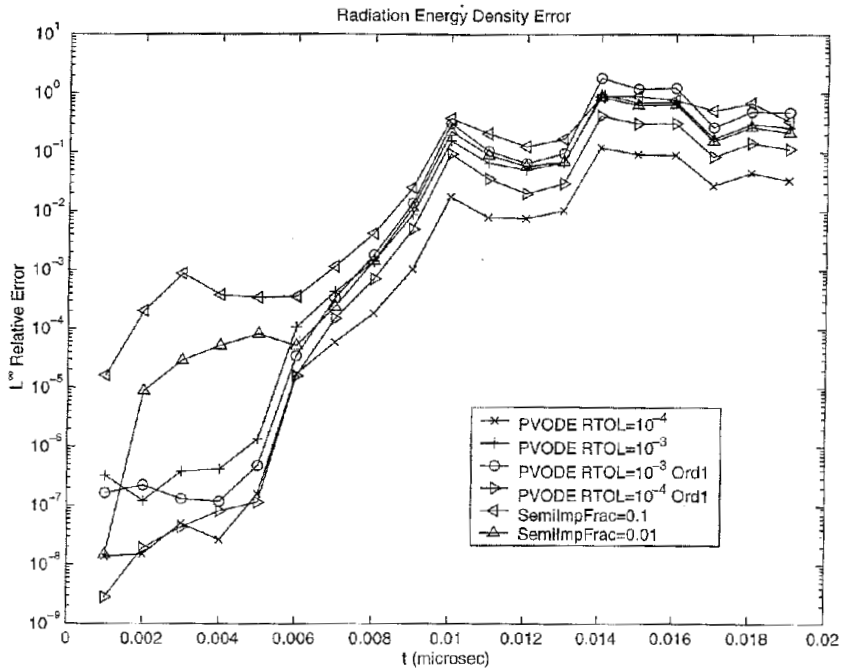

Figure 5: Radiation energy density maximum relative errors (measured against a PVODE run with RTOL= 10^{-5}) for one-dimensional Marshak wave

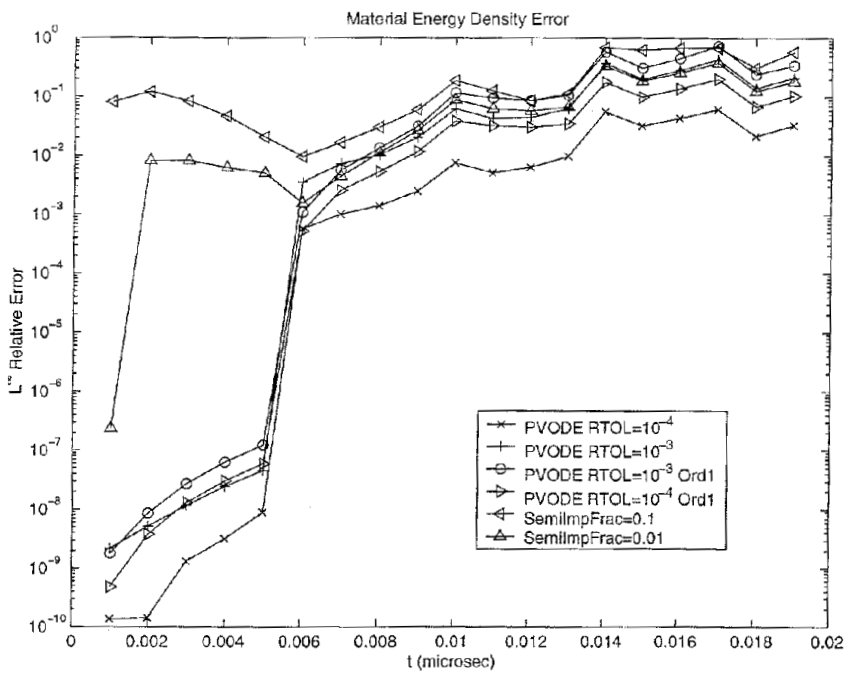

Figure 6: Material energy density maximum relative errors (measured against a PVODE run with RTOL= 10^{-5}) for one-dimensional Marshak wave

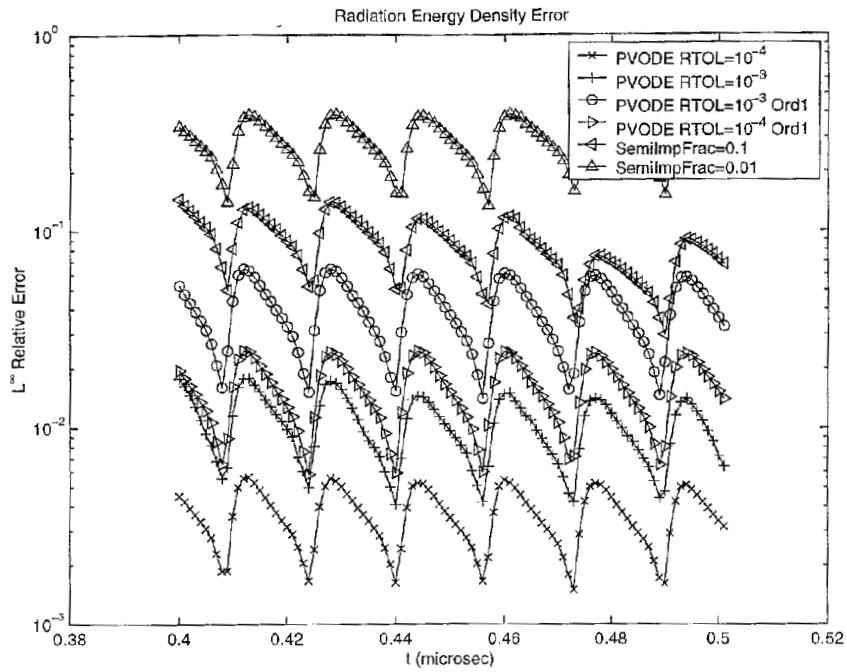

Figure 7: Radiation energy density relative errors (measured against a PVODE run with RTOL= 10^{-5}) for one-dimensional Marshak wave

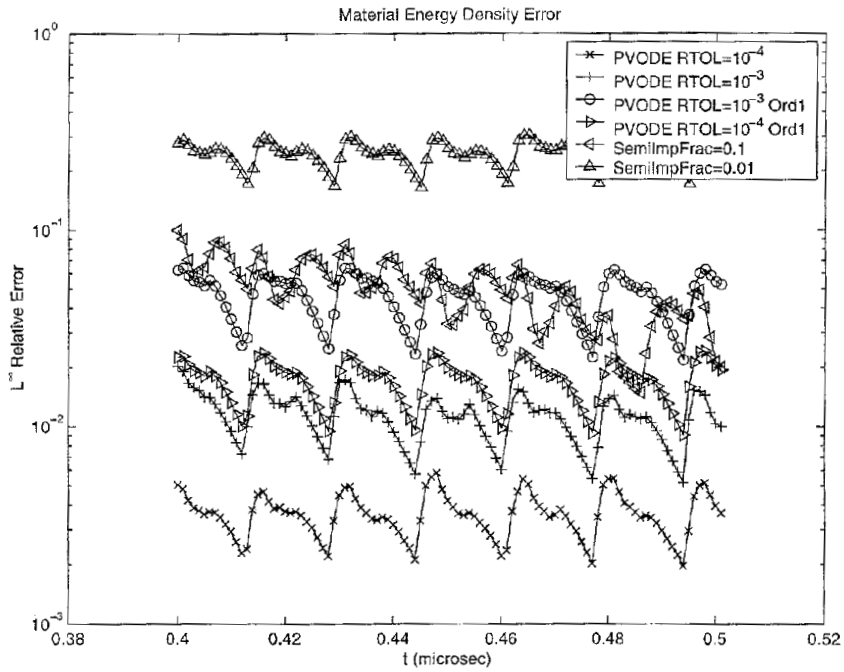

Figure 8: Material energy density maximum relative errors (measured against a PVODE run with RTOL= 10^{-5}) for one-dimensional Marshak wave

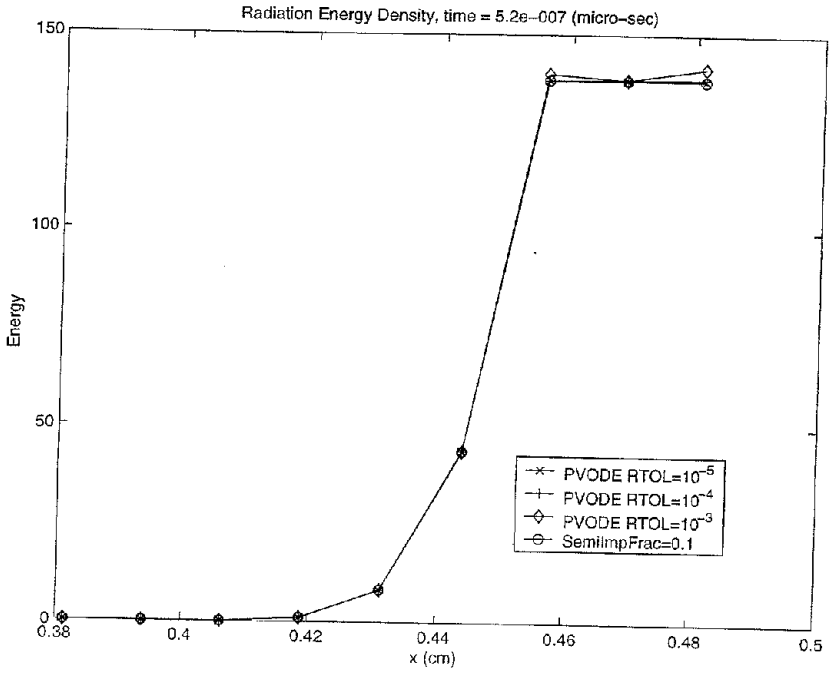

Figure 9: Radiation energy density for three-dimensional problem

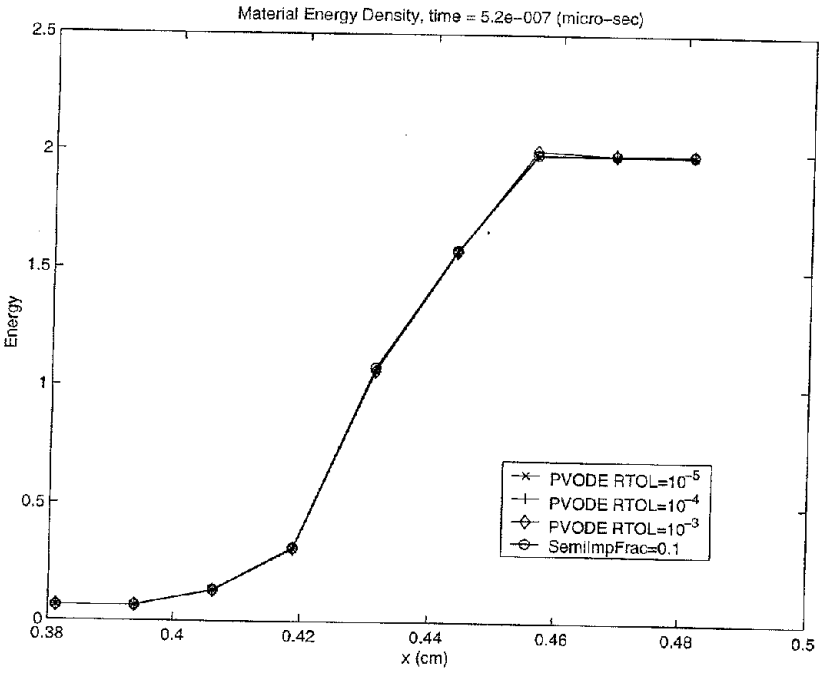

Figure 10: Material energy density for three-dimensional problem

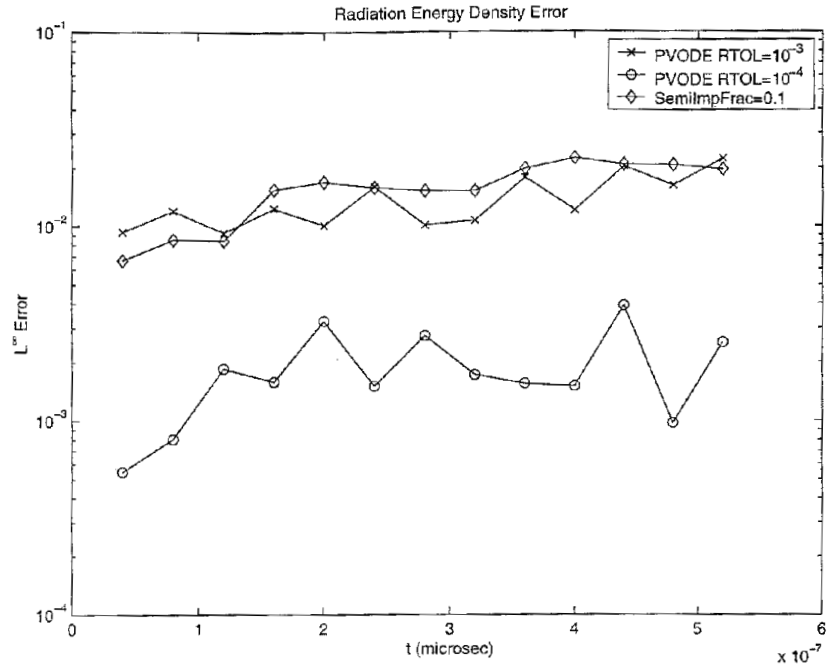

Figure 11: Radiation energy density maximum relative error (measured against a PVODE run with RTOL= 10^{-5}) for three-dimensional Problem

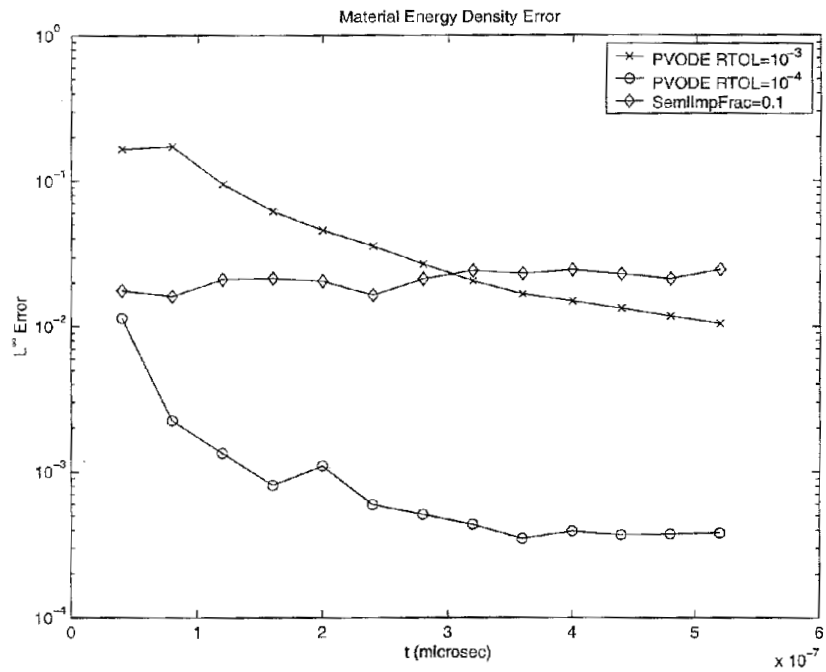

Figure 12: Material energy density maximum relative error (measured against a PVODE run with RTOL= 10^{-5}) for three-dimensional problem